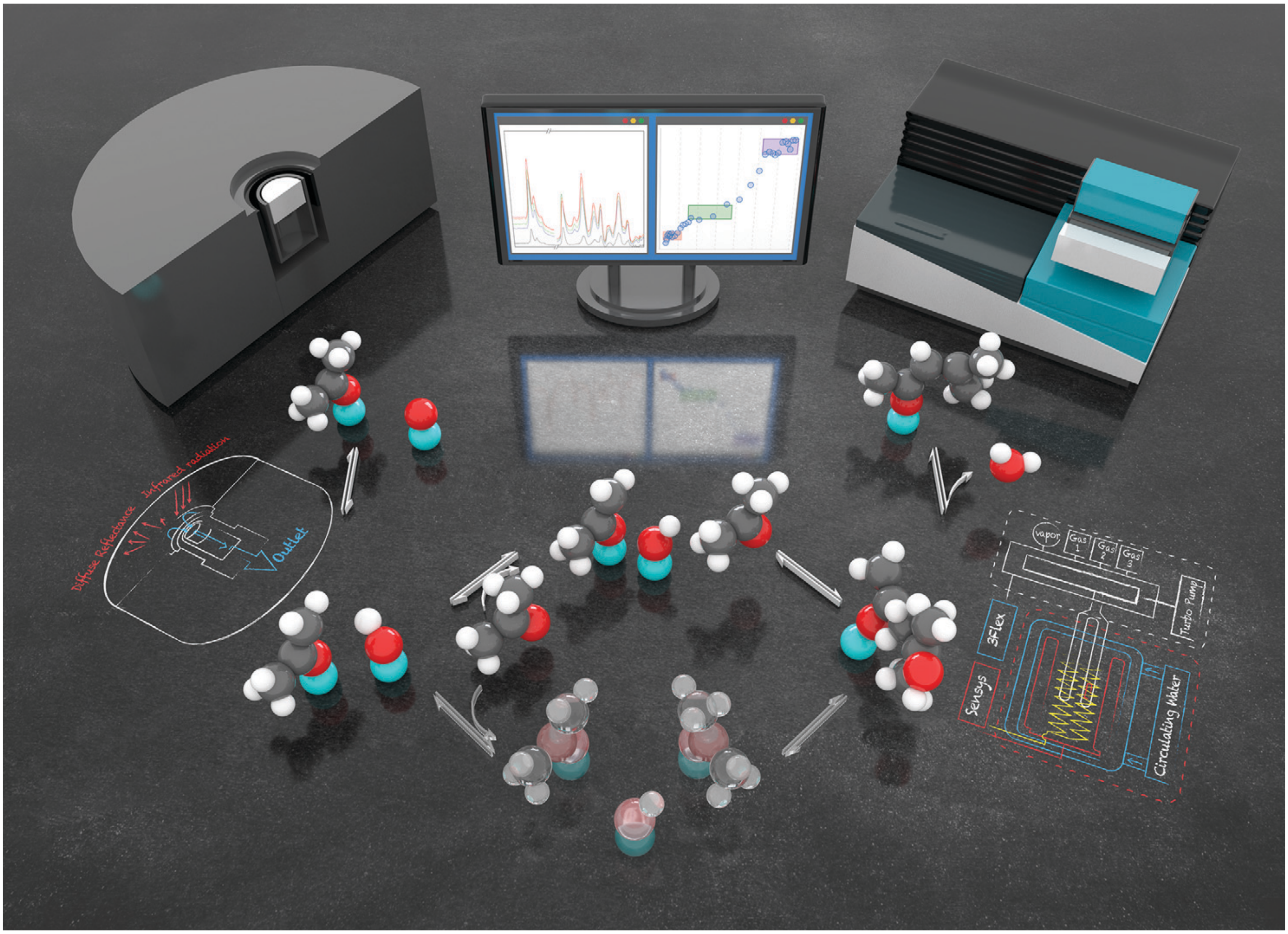

**Showcasing the collaborative research of Dr Yong Wang and his colleagues at Washington State University**

Real-time monitoring of surface acetone enolization and aldolization

Real-time DRIFTS coupled with *in situ* gas adsorption calorimetry reveal the formation of acetone enolate and the subsequent aldolization via an Eley-Rideal type mechanism on the $Zn_1Zr_{10}O_z$.

## As featured in:

Catalysis Science & Technology

See Junming Sun, Yong Wang *et al.*, *Catal. Sci. Technol.*, 2020, **10**, 935.

ROYAL SOCIETY OF CHEMISTRY

rsc.li/catalysis

Registered charity number: 207890

Catalysis
Science &
Technology

ROYAL SOCIETY
OF CHEMISTRY

COMMUNICATION

Check for updates

Cite this: *Catal. Sci. Technol.*, 2020, **10**, 935

Received 18th November 2019,
Accepted 3rd January 2020

DOI: 10.1039/c9cy02339a

rsc.li/catalysis

# Real-time monitoring of surface acetone enolization and aldolization†

Houqian Li,[a] Junming Sun, *[a] Gengnan Li,[a] Di Wu [ab] and Yong Wang*[ac]

**We report the identification of acetone enolate and its subsequent aldolization. The real-time evolution of surface species monitored by *in situ* DRIFTS of surface acetone (-d6) reactions shows clear spectroscopic evidence of the formation of acetone enolate and its subsequent aldolization *via* a dominant Eley–Rideal type mechanism on $Zn_1Zr_{10}O_z$.**

Aldol-condensation (or aldolization) is an extremely important reaction for C–C bond formation in both organic chemistry and heterogeneous catalysis. Aldol-condensation of acetone has been extensively studied in both industry and academia to produce a wide range of valuable chemicals.[1–8] The catalysts studied include both zeolites with Brønsted acidity[3,9] and (mixed) metal oxides with Lewis acid–base pairs.[5,6,10–12] It is generally accepted that both Brønsted acid sites (*i.e.*, protons)[3,9,13] and Lewis acid–base pairs[10,14,15] could activate acetone to produce acetone enolate, a key intermediate in the following aldol addition (C–C formation) reaction.[2,9–12,16–18] Extensive spectroscopic studies, including IR,[10,12,17,19–24] NMR,[9,13,25] XPS,[26] and EELS,[27,28] have been performed in an attempt to identify and isolate the acetone enolate species. The aldol reaction mechanism has also been studied using various methods including kinetic analysis,[18,29] IR,[10] NMR,[25] and DFT[30] to distinguish whether the products are formed *via* the Langmuir–Hinshelwood (L–H) or the Eley–Rideal (E–R) mechanism. Despite the extensive studies on the identification of acetone enolate over metal oxide catalysts with Lewis acid–base site pairs,[21,23,27] there are still ongoing debates whether the reported acetone enolate[19] is an acetate[20] or aldol adduct (*i.e.*, mesityl oxide).[10] Moreover, no definitive evidence was reported regarding C–C bond formation following the L–H or the E–R mechanism.

We have recently shown that balanced Lewis acid–base site pairs on $Zn_1Zr_{10}O_z$ are highly selective and stable for acetone aldolization and self-deoxygenation reactions to selectively produce isobutene.[5,31] Although the specific role of framework $Zn^{2+}$ has been addressed in these particular cascade reactions, the formation of the acetone enolate intermediate and its subsequent aldol reaction mechanism remain elusive. Herein, we use *in situ* DRIFTS with a modulated gas delivery system to control the surface acetone supply. As a result, a complicated sequential aldol reaction could be deconvoluted, and thus acetone enolate and its subsequent aldolization reactions are successfully monitored. Complemented with gas/vapor adsorption calorimetry, we provide for the first time experimental evidence showing insightful reaction mechanisms of the adsorption of acetone

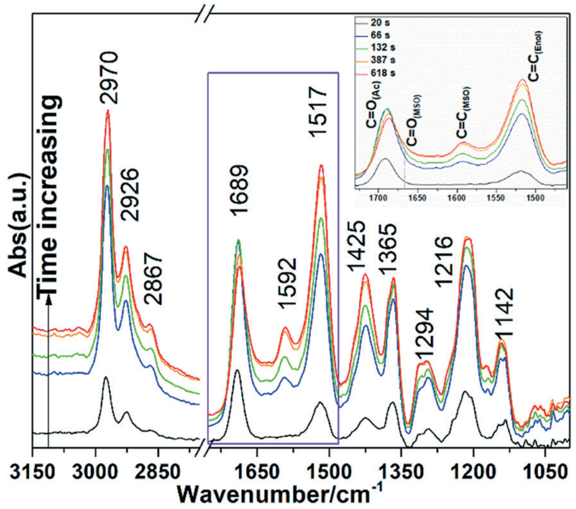

**Fig. 1** Evolution of infrared spectra of adsorbed acetone *vs.* time on $Zn_1Zr_{10}O_z$ after the 1st dose; (inset) zoom-in spectra marked in Fig. 1. Each spectrum takes ~20 s (32 scans). Adsorption experiments were done at 25 °C.

---

[a] *The Gene & Linda Voiland School of Chemical Engineering and Bioengineering, Washington State University, Pullman, WA 99164, USA. E-mail: junming.sun@wsu.edu*
[b] *Alexandra Navrotsky Institute for Experimental Thermodynamics, Washington State University, Pullman, WA 99164, USA*
[c] *Institute for Integrated Catalysis, Pacific Northwest National Laboratory, Richland, WA 99352, USA. E-mail: yong.wang@pnnl.gov*

† Electronic supplementary information (ESI) available. See DOI: 10.1039/c9cy02339a

as well as the subsequent elementary surface reactions (*i.e.*, enolization, C–C coupling *via* aldolization).

The unique Zr–O–Zn surface structure and Lewis acid–base properties of $Zn_xZr_yO_z$ have been reported elsewhere.[5,15,31] In this work, the surface acetone reactions are mainly focused on $Zn_1Zr_{10}O_z$ with Zr–O–Zn Lewis acid–base site pairs.[31] During acetone adsorption on $Zn_1Zr_{10}O_z$, if the acetone supply is not controlled, acetone enolization on the catalyst surface and subsequent aldolization occur rapidly, establishing surface equilibrium where surface mesityl oxide and unreacted acetone dominate the surface and the acetone enolate intermediate can barely be observed.[5] From this study, the infrared spectra of acetone were found to be dependent on the amount/surface coverage of acetone (controlled by the number of doses) and the time span between doses. The surface activation especially the subsequent aldol reactions was interrupted by these conditions, causing the observation of acetone enolate. Fig. 1 shows the evolution of infrared spectra with time on $Zn_1Zr_{10}O_z$ after the 1st dose of acetone. Peaks characteristic of acetone adsorption on Lewis acid sites can be observed at 1689 $cm^{-1}$ ($\nu$(C═O)), 1365 $cm^{-1}$ ($\delta_s(CH_3)$), and 1216 $cm^{-1}$ ($\nu$(C–C)) after ~20 s of acetone dosing (Fig. 1, black line).[10,11] Weakly adsorbed acetone on surface hydroxyl groups is minimum at >1700 $cm^{-1}$. Notably, another set of bands is clearly discerned at 1517 $cm^{-1}$, 1425 $cm^{-1}$, 1313 $cm^{-1}$, and 1142 $cm^{-1}$, which can be assigned to the $\nu$(C═C), $\delta_a(CH_3)/\delta({=}CH_2)$, $\nu$(C–O), and $\rho(CH_2)$ of the acetone enolate, respectively.

Note that the peaks at 1517 $cm^{-1}$ and 1425 $cm^{-1}$ could also be ascribed to the vibration of $\nu_a$(OCO) and $\nu_s$(OCO) of acetate or poly-acetone species, respectively. These have been observed on rutile $TiO_2$.[23,28] To further confirm the peak assignment, *in situ* DRIFTS of adsorbed acetone-d6 was performed (Fig. 2). If the peaks at 1517 $cm^{-1}$ and 1425 $cm^{-1}$ are indeed contributed by the acetate or poly-acetone species, their peak positions should not be affected by deuterated isotope labelling, and *vice versa* for the peak at 1425 $cm^{-1}$ ($\delta_a(CH_3)/\delta({=}CH_2)$). It has been observed that fast H–D exchange occurs between acetone and surface hydroxyl groups over $Zn_xZr_yO_z$.[5] To minimize the effect of surface H of $Zn_xZr_yO_z$, $D_2O$ is first used to remove the H from the surface hydroxyl groups of the catalyst before the adsorption of acetone-d6.[5] Fig. 2 shows the time evolution of infrared spectra after the 1st dose of acetone-d6 over the deuterated $Zn_xZr_yO_z$. From the region of 1000–1800 $cm^{-1}$ (Fig. 2), both deuterated enolate and MSO are observed, and the intensity increases at the expense of acetone-d6. However, all the peaks shifted at different extents. For deuterated enolate species, as expected, the $\nu$(C═C) and $\nu$(C–O) bands shifted marginally ($\nu_{H/D}$ = 1.02) from 1517 $cm^{-1}$ and 1313 $cm^{-1}$ to 1488 $cm^{-1}$ and 1296 $cm^{-1}$, respectively. The peaks at 1425 $cm^{-1}$ shifted significantly ($\delta_{H/D}$ = 1.32) to 1082 $cm^{-1}$, and the peak at 1365 $cm^{-1}$ was split into two with one shifted to 1036 $cm^{-1}$ and another to 1356 $cm^{-1}$. The peak at 1356 $cm^{-1}$ could be due to the $\delta_s$(CH) exchanged from the residue surface OH on the catalyst, or the vibration mode that is not C–H related. For the deuterated MSO, the $\nu$(C═C) and $\nu$(C═O) bands also slightly shifted from 1592 $cm^{-1}$ and ~1665 $cm^{-1}$ to 1576 $cm^{-1}$ and 1645 $cm^{-1}$, respectively. Nevertheless, the results suggest that the peaks at 1517 $cm^{-1}$ and 1425 $cm^{-1}$ should belong to the vibrations of $\nu$(C═C) and $\delta_a(CH_3)/\delta({=}CH_2)$ of acetone enolate, rather than the $\nu_a$(OCO) and $\nu_s$(OCO) vibrations of acetate or poly-acetone.

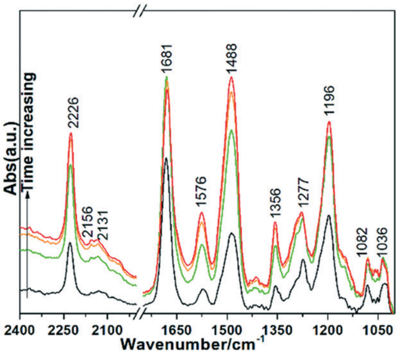

**Fig. 2** Evolution of infrared spectra of adsorbed acetone-d6 on deuterated $Zn_1Zr_{10}O_z$ after one dose. Each spectrum takes ~20 s (32 scans). Adsorption experiments were done at 25 °C.

The evolving spectra reveal rapid changes of surface species with time. Specifically, the intensity of the peak corresponding to the adsorbed acetone (1689 $cm^{-1}$) first increases and then decreases with time, whereas the peak intensity of acetone enolate (1517 $cm^{-1}$) increases monotonically (Fig. 1, inset). In addition, a small amount of surface mesityl oxide (MSO) appears at ~66 s (Fig. 1, red line) and its amount increases slightly with time, evidenced by the characteristic $\nu$(C═C) vibration bands at 1592 $cm^{-1}$, as well as the shoulders at 1665 $cm^{-1}$ ($\nu$(C═O)), 1450 $cm^{-1}$ ($\rho$(C–H)), and 1255/1225 $cm^{-1}$ ($\nu$(C–C)),[10] which can be further confirmed by separate DRIFTS analysis of adsorbed MSO on the $Zn_1Zr_{10}O_z$ catalysts (Fig. S3†). Note that a slight red shift in C═O stretching (Fig. 1, inset) was observed with time, likely caused by the increasing MSO C═O shoulder band at 1665 $cm^{-1}$. The formation of a small amount of MSO suggests that, although it is not dominant, the subsequent aldolization reaction takes place on the $Zn_1Zr_{10}O_z$ catalyst even at a low coverage (*i.e.*, ~0.11 monolayer), which will be further discussed in the following section. No detectable diacetone alcohol is observed, suggesting that the subsequent dehydration of diacetone alcohol is kinetically more favourable than the C–C coupling reaction.

After the surface reaches equilibrium evidenced by the relatively stable evolving spectra, another dose of acetone is added, and the evolution of spectra with time is continuously monitored by DRIFTS. The process is repeated for a total of 5 doses, and the spectra are plotted in Fig. S5–S8.† In order to better understand the evolution of the different surface species, a peak integration and semi-quantitative comparison is performed. The unique $\nu$(C═C) bands at 1517 $cm^{-1}$ and 1592 $cm^{-1}$ (Fig. 1, inset) were integrated to represent surface acetone enolate and MSO, respectively. Given that the $\nu$(C═O) bands of adsorbed acetone and MSO overlap at ~1689 $cm^{-1}$, a careful peak deconvolution/integration was done to isolate the contribution of surface adsorbed acetone (Table S1 and Fig. S2 and S4†). The evolution of surface acetone, acetone enolate and MSO is plotted as a function of time and dose, as shown in Fig. 3. Overall, the acetone enolate reaches a maximum at the 2nd dose, after which it decreases. Surface MSO increases monotonically with the number of doses. Clearly, the subsequently added acetone consumes surface acetone enolate *via* the aldolization reaction, forming MSO that adsorbs and accumulates on the surface Lewis acid sites at 25 °C. Consistent with this observation, our online MS does not detect any gas phase MSO (Fig. S9†).

For the evolution of each species after a dose, surface adsorbed acetone showed a rapid increase then decreased slowly with time after the 1st dose (Fig. 3). The observation of maximum surface acetone is due to a combination effect of adsorption/desorption of gas phase acetone followed by depletion *via* the subsequent conversion of surface acetone to enolate and then to MSO. Indeed, the surface acetone enolate is observed and increases monotonically at the expense of acetone. The amount of surface MSO, however, increases rapidly only within a given period of ~150 s, after which it remains relatively constant with time irrespective of the decreasing surface acetone. This observation suggests that, after the 1st dose (*i.e.*, at low surface acetone coverage), the adsorbed acetone molecules on the surface Lewis acid sites are mainly activated to form surface acetone enolate, and those non-activated acetone molecules are barely involved in the aldol reactions with surface acetone enolate, otherwise surface MSO will increase with time. The results indicate that MSO formation may not follow the Langmuir–Hinshelwood mechanism (L–H mechanism, a reaction between surface acetone enolate and adsorbed acetone, gray highlighted in Scheme 1). Additionally, given the sufficient evolving time after the admission, not all the adsorbed surface acetone is converted into enolate. It suggests that either the surface is equilibrated or only some of the stronger surface Lewis acid–base site pairs are active for acetone enolization under the studied conditions (*i.e.*, room temperature).

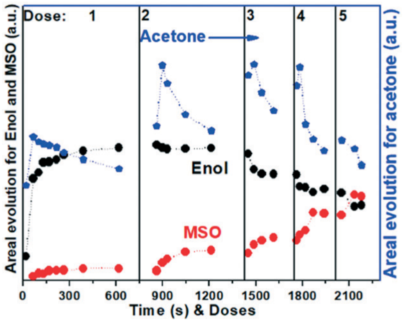

**Fig. 3** Semi-quantitative evolution of the amount of surface acetone, acetone enolate, and mesityl oxide on $Zn_1Zr_{10}O_z$ as a function of time and dose.

After the 2nd dose, surface acetone shows a similar initial rapid increase and then decreases at a much higher extent than the 1st one. The stabilized surface acetone amount is also higher than that of the 1st dose (Fig. 3, 600 s *vs.* 1200 s) for the increased surface coverage. Interestingly, the surface acetone enolate seemingly saturated with no observable changes, whereas the surface MSO shows a similar initial rapid increase within ~150 s after the 2nd acetone admission, and then levels off with time. Most importantly, during the time span when MSO remains constant, the surface acetone keeps decreasing significantly. This similar behaviour is also observed during the following doses, especially at 4–5 doses (*i.e.*, at high surface acetone coverages close to the reaction conditions). It further suggests that, under reaction conditions, the adsorbed acetone (including those weakly adsorbed) is not directly involved in the aldol-condensation producing surface MSO (otherwise the surface MSO should increase at the expense of acetone). Instead, those seem rapidly desorbed and purged into the deep side of the sample holder where the gas-phase acetone may either further react with the surface enolate to form MSO though undetectable by IR (Fig. S1†), or those are directly flushed into the downstream gas phase evidenced by our online MS (Fig. S9†). Noteworthily, our separate blank experiment reveals that the system has a gas holdup time of ~135 s for acetone (data not shown), and this time span matches the MSO formation time (150 s) after each acetone admission. This observation reveals that the formation of MSO occurs only when gas phase acetone is present. In other words, the aldolization predominantly go through a fast bimolecular reaction between the surface acetone enolate and gas phase acetone (*i.e.*, E–R mechanism, Scheme 1). To the best of our knowledge, this is the first spectroscopic evidence showing the surface acetone aldolization reaction mechanism.

It should be noted that, regardless of surface acetone coverage, acetone enolate is barely observed (Fig. S10†) on $ZrO_2$, which is different from $Zn_1Zr_{10}O_z$. This result suggests that α-H abstraction is kinetically relevant on $ZrO_2$. The kinetically relevant α-C–H bond cleavage was also observed in alkanal/alkanone enolization on $ZrO_2$.[29] The fact that a substantial amount of acetone enolate is observed on $Zn_1Zr_{10}O_z$ rather than on $ZrO_2$ suggests that Zr–O–Zn indeed shows enhanced Lewis basicity, which in turn accelerates the α-H abstraction of acetone (*i.e.*, enolization reaction) *via* a likely favourable hydrogen transfer.[5]

To further our understanding on the complex molecular acetone interactions and reactions revealed by *in situ* DRIFTS, we carried out acetone adsorption calorimetry on the same $Zn_1Zr_{10}O_z$ catalyst at 25 °C. Adsorption calorimetry has been primarily applied to investigate the energetics of complex gas–solid surface interactions.[32,33] Acetone adsorption on the metal oxide surface with Lewis acid–base pairs is extremely complicated with simultaneous surface activation and reaction occurring even at room temperature.[11,12,19,22,33] Therefore, the energetic effects recorded may include contributions from not only the adsorption but also the subsequent

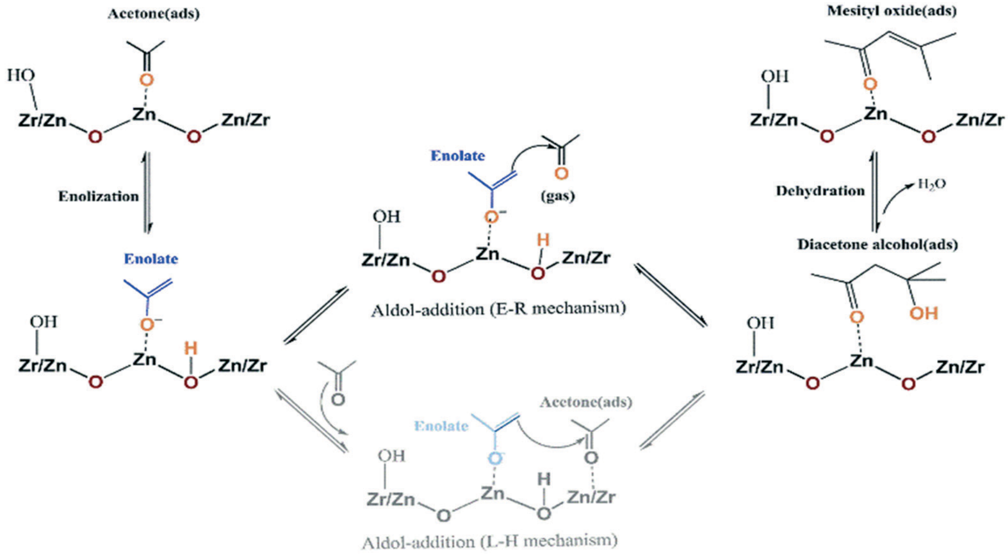

**Scheme 1** Proposed reaction pathway for acetone aldolization on the $Zn_1Zr_{10}O_z$.

enolization and even further aldol reactions. Typically, such complicated energetic effects were not considered during the calorimetric measurement of acetone adsorption on metal oxides.[34] Acetone adsorption on the $Zn_1Zr_{10}O_z$ catalyst results in a type II isotherm (Fig. S11†), suggesting favourable acetone–surface interaction. Fig. 4 shows the corresponding differential enthalpies of the adsorption/reaction curve as a function of acetone introduced, which presents three distinct energetic plateaus. At near-zero coverage, an initial adsorption enthalpy of −117 kJ mol$^{-1}$ acetone is observed. Subsequently, the differential enthalpy of adsorption curve tends to be less exothermic and reaches the first plateau at about −110 kJ mol$^{-1}$ ending at ~0.10 mmol$_{ace}$ g$_{cat.}$$^{-1}$, which is roughly 1/3 coverage of the surface of the $Zn_1Zr_{10}O_z$ catalyst. Further acetone uptake leads to weaker adsorbate–adsorbent interactions, and the differential enthalpy of adsorption profile levels off at its second plateau at about −90 kJ mol$^{-1}$ acetone (concluding at about 0.4 mmol acetone per g$_{cat}$). Eventually, the differential adsorption enthalpy gradually becomes less exothermic and reach its final plateau at −30 kJ mol$^{-1}$ corresponding to weak intermolecular interactions (such as condensation) on the $Zn_1Zr_{10}O_z$ surface at 25 °C.

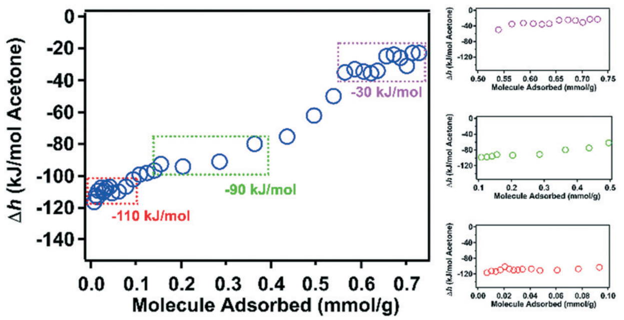

**Fig. 4** The differential enthalpies of adsorption as a function of acetone loading at 25 °C, in which stepwise energetic profile was observed.

Together with the *in situ* DRIFTS analysis, it is proposed that the acetone adsorption and enolization are dominant at low surface coverages. The differential enthalpy of acetone adsorption measured at the first plateau (−110 kJ mol$^{-1}$) appears to be mainly generated from acetone adsorption and enolization. At higher coverage, other than acetone adsorption and enolization, surface aldolization reactions occur and start to dominate, which may lead to the second plateau (≃90 kJ mol$^{-1}$). The 20 kJ mol$^{-1}$ difference between the two plateaus at different coverages probably indicates the contribution of endothermic surface acetone aldolization (aldol addition and dehydration) reactions at higher acetone doses (*i.e.*, 0.10–0.45 mmol acetone per g$_{cat}$). Given that the generated MSO is strongly adsorbed on the surface, further increasing the acetone dosage results in the saturation of surface active sites. Therefore, the directly measured enthalpy of adsorption profiles concludes at about −30 kJ mol$^{-1}$, where only acetone–acetone or acetone–MSO intermolecular interactions exist.

By starving the catalyst surface (*i.e.*, controlling the surface acetone supply), our *in situ* DRIFTS coupled with gas adsorption calorimetry not only successfully isolated the surface enolate, but also observed the subsequent aldol reactions in real time. For the first time, we show spectroscopic evidence of acetone enolate formation and the subsequent aldolization *via* the dominant E–R mechanism.

## Conflicts of interest

There are no conflicts to declare.

## Acknowledgements

The authors acknowledge the U.S. Department of Energy (DOE), Office of Basic Energy Sciences, Division of Chemical Sciences, Biosciences and Geosciences (DE-AC05-RL01830, FWP-47319, DE-SC0014560) and Shandong Chambroad

Holding Company. Di Wu acknowledges the fund of Alexandra Navrotsky Institute for Experimental Thermodynamics.

## Notes and references

1 G. S. Salvapati, K. V. Ramanamurty and M. Janardanarao, *J. Mol. Catal.*, 1989, **54**, 9–30.
2 L. Faba, E. Diaz and S. Ordonez, *Appl. Catal., B*, 2013, **142**, 387–395.
3 G. J. Hutchings, P. Johnston, D. F. Lee, A. Warwick, C. D. Williams and M. Wilkinson, *J. Catal.*, 1994, **147**, 177–185.
4 A. A. Nikolopoulos, B. W. L. Jang and J. J. Spivey, *Appl. Catal., A*, 2005, **296**, 128–136.
5 J. M. Sun, R. A. L. Baylon, C. J. Liu, D. H. Mei, K. J. Martin, P. Venkitasubramanian and Y. Wang, *J. Am. Chem. Soc.*, 2016, **138**, 507–517.
6 J. Quesada, L. Faba, E. Díaz, S. Bennici, A. Auroux and S. Ordóñez, *J. Catal.*, 2015, **329**, 1–9.
7 Z. Wang, P. Fongarland, G. Z. Lu and N. Essayem, *J. Catal.*, 2014, **318**, 108–118.
8 J. Sun and Y. Wang, *ACS Catal.*, 2014, **4**, 1078–1090.
9 T. Xu, E. J. Munson and J. F. Haw, *J. Am. Chem. Soc.*, 1994, **116**, 1962–1972.
10 A. G. Panov and J. J. Fripiat, *J. Catal.*, 1998, **178**, 188–197.
11 M. I. Zaki, M. A. Hasan and L. Pasupulety, *Langmuir*, 2001, **17**, 768–774.
12 M. I. Zaki, M. A. Hasan, F. A. Al-Sagheer and L. Pasupulety, *Langmuir*, 2000, **16**, 430–436.
13 A. I. Biaglow, J. Sepa, R. J. Gorte and D. White, *J. Catal.*, 1995, **151**, 373–384.
14 V. Crocella, G. Cerrato and C. Morterra, *Phys. Chem. Chem. Phys.*, 2013, **15**, 13446–13461.
15 H. Li, J. Sun and Y. Wang, *Appl. Catal., A*, 2019, **573**, 22–31.
16 G. Zhang, H. Hattori and K. Tanabe, *Appl. Catal.*, 1988, **40**, 183–190.
17 R. King and H. Idriss, *Langmuir*, 2009, **25**, 4543–4555.
18 S. Herrmann and E. Iglesia, *J. Catal.*, 2017, **346**, 134–153.
19 H. Miyata, Y. Toda and Y. Kubokawa, *J. Catal.*, 1974, **32**, 155–158.
20 B. E. Hanson, L. F. Wieserman, G. W. Wagner and R. A. Kaufman, *Langmuir*, 1987, **3**, 549–555.
21 W. S. Sim, T. C. Li, P. X. Yang and B. S. Yeo, *J. Am. Chem. Soc.*, 2002, **124**, 4970–4971.
22 J. F. Sanz, J. Oviedo, A. Marquez, J. A. Odriozola and M. Montes, *Angew. Chem., Int. Ed.*, 1999, **38**, 506–509.
23 T. Würger, W. Heckel, K. Sellschopp, S. Müller, A. Stierle, Y. Wang, H. Noei and G. Feldbauer, *J. Phys. Chem. C*, 2018, **122**, 19481–19490.
24 Y. Jing, Y. Xin, Y. Guo, X. Liu and Y. Wang, *Chin. J. Catal.*, 2019, **40**, 1168–1177.
25 J. D. Lewis, S. Van de Vyver and Y. Roman-Leshkov, *Angew. Chem., Int. Ed.*, 2015, **54**, 9835–9838.
26 J. M. Vohs and M. A. Barteau, *J. Phys. Chem.*, 1991, **95**, 297–302.
27 C. R. Ayre and R. J. Madix, *J. Am. Chem. Soc.*, 1995, **117**, 2301–2312.
28 M. A. Henderson, *J. Phys. Chem. B*, 2004, **108**, 18932–18941.
29 S. Wang and E. Iglesia, *J. Phys. Chem. C*, 2016, **120**, 21589–21616.
30 D. Palagin, V. L. Sushkevich and I. I. Ivanova, *J. Phys. Chem. C*, 2016, **120**, 23566–23575.
31 R. A. L. Baylon, J. M. Sun, L. Koyarik, M. Engelhard, H. Q. Li, A. D. Winkelman and Y. Wang, *Appl. Catal., B*, 2018, **234**, 337–346.
32 D. Wu, X. F. Guo, H. Sun and A. Navrotsky, *J. Phys. Chem. C*, 2016, **120**, 7562–7567.
33 V. Crocellà and C. Morterra, *J. Phys. Chem. C*, 2010, **114**, 18972–18987.
34 M. Li and J. Shen, *J. Catal.*, 2002, **205**, 248–258.